ACS APPLIED MATERIALS & INTERFACES

www.acsami.org

Research Article

200-Fold Lifetime Extension of 2,6- Dihydroxyanthraquinone Electrolyte during Flow Battery Operation

Meisam Bahari, Yan Jing, Shijian Jin, Marc-Antoni Goulet, Tatsuhiro Tsukamoto, Roy G. Gordon, and Michael J. Aziz*

Cite This: *ACS Appl. Mater. Interfaces* 2024, 16, 52144−52152

Read Online

ACCESS | Metrics & More | Article Recommendations | Supporting Information

ABSTRACT: We study the capacity fade rate of a flow battery utilizing 2,6-dihydroxyanthraquinone (DHAQ) and its dependence on hydroxide concentration, state of charge, cutoff voltages for the discharge step and for the electrochemical regeneration (oxidation of decomposition compounds back to active species) step, and the period of performing the electrochemical regeneration events. Our observations confirm that the first decomposition product, 2,6-dihydroxyanthrone (DHA), is stable, but after electro-oxidative dimerization, the anthrone dimer decomposes. We identify conditions for which there is little time after dimerization until the dimer is rapidly reoxidized electrochemically to form DHAQ. Combining these approaches, we decrease the fade rate to 0.02%/day, which is 18 times lower than the lowest rate reported previously of 0.38%/day, and over 200 times lower than the value under standard cycling conditions of 4.3%/day. The findings and their mechanistic interpretation are expected to extend the lifetime and enhance the effectiveness of in situ electrochemical regeneration for other electroactive species with finite lifetimes.

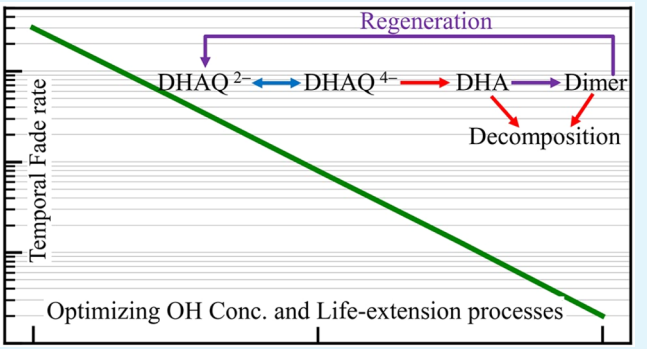

KEYWORDS: *aqueous organic flow battery, extending lifetime, alkaline flow battery, anthraquinone, DHAQ, decomposition, electrochemical regeneration, state of charge restriction*

INTRODUCTION

Although the cost of emissions-free electricity from photovoltaics and wind power has dropped below the cost of fossil fuel-generated electricity, the intermittency of these renewable resources presents an increasingly difficult problem as their contribution to the generation mix grows.[1] One potential solution is storing energy from these sources when available and then using it when necessary. In addition to utilizing renewable sources, stationary storage also plays a significant role in balancing the power supply and demand for grid electricity.[2]

Various energy storage systems have been developed so far, among which flow batteries are particularly suitable for grid storage needs.[3] The unique architecture of flow batteries makes it possible to decouple power and energy scaling, offering system flexibility to fit a wide range of specifications for power and discharge duration, i.e., energy/power ratio. Aqueous flow batteries, in particular, utilize water as the solvent and have no flammability concern.[4] Operating in water also has a significant cost advantage. Aqueous-soluble organic energy-storing molecules, benefiting from structural diversity and the earth abundance of their atomic components, may permit scalable, safe, cost-effective long-duration energy storage in aqueous redox flow batteries.[5−7]

From the cost perspective, one of the promising energy storage molecular families is that of anthraquinone derivatives,[8−11] such as 2,6-dihydroxyanthraquinone ($DHAQ^{2-}$ or DHAQ for simplicity),[12] whose cost is low at a mass production scale (~$4/kg).[13] However, the main challenge of utilizing DHAQ as the negolyte (negative electrolyte) species is its fast decomposition rate, caused by the instability of reduced DHAQ ($DHAQ^{4-}$). The decomposition mechanism of $DHAQ^{4-}$ has been identified, and two strategies for reducing and reversing this decomposition have been demonstrated.[14−16] The first strategy involves restricting the state of charge (SOC) of the negolyte.[14] The second approach is to electrochemically oxidize the decomposition product, 2,6-dihydroxyanthrone (DHA), back into DHAQ.[16] The latter approach involves lowering the cell voltage during the discharge step to values where the negolyte, specifically the decomposition products, experiences a potential that is more

Received: April 14, 2024
Revised: September 9, 2024
Accepted: September 13, 2024
Published: September 24, 2024

positive than that in normal cycling. As a result, the side products are oxidized back to DHAQ.

A flow battery utilizing DHAQ exhibits a temporal fade rate of ∼4.3%/day (measured in this study) under normal cycling conditions. When the electrochemical regeneration strategy is implemented, a fade rate of 0.38%/day is reported, which is over an order of magnitude improvement.[16] However, this fade rate is still very fast, preventing DHAQ from being an attractive negolyte species for commercialization purposes, despite its low predicted cost of manufacture. This study aims to explore the possibility of further reducing the fade rate. Thus, the effects of various factors that may affect the effectiveness of the electrochemical regeneration technique and the fade rate are investigated. These factors are the concentration of OH^-, the cutoff voltage of the discharge step in normal cycling, the cutoff voltage of the regeneration step, and the period of the periodic regeneration events. Properly controlling these factors combined with restricting the negolyte SOC to 0−85% leads to a fade rate as low as 0.02%/day, which is over 200 times lower than that under standard cycling conditions. The findings and mechanistic insights obtained in this study are anticipated to improve the effectiveness of in situ electrochemical regeneration for other electroactive species with finite lifetimes.

MATERIALS AND METHODS

Chemical Characterization. Ex situ ^1H NMR spectra were recorded on a Varian INOVA 500 spectrometer at 500 MHz. Aliquots were taken and put in D_2O, and the corresponding NMR spectra were recorded in D_2O. Liquid chromatography−mass spectrometry (LC−MS) was conducted on a Bruker microTOF-QII mass spectrometer. 150 ul aliquots were taken and by water/acetonitrile (v/v = 1:1) to the desired concentration (∼10 μM) before LC−MS measurements.

Material Synthesis. DHA(L) was synthesized as described in ref 14. In brief, DHAQ and excess stannous chloride were refluxed for 7 h in concentrated HCl. The resulting solution was cooled to room temperature, and the precipitate was collected by vacuum filtration. The collected solid was washed with deionized water and then dried in vacuo to afford a pale-yellow powder.

Materials. Potassium hydroxide, potassium ferrocyanide, and potassium ferricyanide were purchased from Sigma-Aldrich. 2,6-Dihydroxyanthraquinone (DHAQ) was purchased from Carbosynth. All of these reagents were used with no further purification.

Flow Cell Setup. Flow cell experiments were constructed with cell hardware from Fuel Cell Tech or an in-house cell with end plates made from PVC. Both designs were assembled into a zero-gap flow cell configuration using either pyrosealed POCO graphite flow plates or resin-impregnated carbon flow plates from MWI with identical interdigitated flow fields. Each electrode comprised one layer of Zoltek PXFB carbon cloth with a geometric surface area of 5 cm^2. Nafion 117 membranes presoaked in 1 M KOH for at least 24 h were used in all cell cycling tests.

The torque applied during cell assembly was 60 lb-in (for Fuel Cell Tech cells) or 25 lb-in (for in-house cells) on each of eight 3/8″-24 bolts. The electrolytes were fed into the cell through fluorinated ethylene propylene (FEP) tubing at a rate of 60 mL/min, controlled by ColeParmer 6 Masterflex L/S peristaltic pumps or KNF diaphragm liquid pumps (FF 12 DCB-4).

All flow cell experiments were set up inside a N_2-filled glovebox (Vacuum Atmospheres Company) with <5 ppm of oxygen and were cycled at room temperature. The alkalinity of the electrolytes was made exclusively using KOH. All of the KOH concentrations reported for the negolytes are the excess KOH concentration (in addition to what is required for the deprotonation of the active species).

Reference Electrode (RE). To independently track the voltage of the negative electrode in flow cell experiments, as presented in Figure 3, a Hg/HgO RE (BASi, with an internal electrolyte of 1 M KOH) was positioned externally on the inlet of the negolyte stream. The RE was inserted in a two-compartment holder one side of which contained the supporting electrolyte (1−2 M KOH depending on the experiment) and through the other side the negolyte flowed. The two compartments were separated using a Nafion 117 membrane. RE was inserted in the side that contained the supporting electrolyte; this strategy prevented the diffusion of the active material in the RE itself to ensure a stable RE over long term. Figure S7 shows how the reference electrode was positioned.

RESULTS AND DISCUSSION

pH Effect. The impact of pH on the fade rate has been reported before.[17] However, hydroxide concentrations of >1.0 M have rarely been examined. Figure 1a shows the time

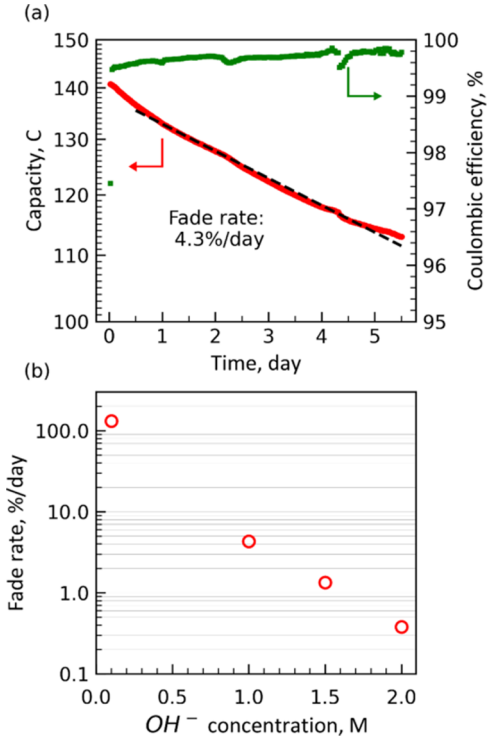

Figure 1. (a) Semilog plot of discharge capacity and Coulombic efficiency vs time for a DHAQ | ferro/ferricyanide full cell in 1 M OH^- (KOH). (b) Fade rate as a function of OH^- (KOH) concentration. Test conditions: negolyte contained 7−7.5 mL of 0.1 M DHAQ, and the posolyte consisted of 50 mL of 0.06 M potassium ferrocyanide and 0.03 M potassium ferricyanide. Cycling was performed under constant current density at 50 mA/cm^2 followed by a potentiostatic hold. Cutoff voltages for the charge and discharge steps were 1.4 and 0.9 V, respectively. Cutoff current densities for the charge and discharge steps were 2 and 1 mA/cm^2, respectively.

dependence of the discharge capacity of a cell that contains 0.1 M DHAQ in the negolyte and 0.06/0.03 M ferrocyanide/ferricyanide in the posolyte in 1.0 M OH^-. Similar tests were performed at various OH^- concentrations and the fade rates are shown in Figure 1b (for the definition of fade rate, refer to the SI, Section 1.1). Increasing the OH^- concentration over the range 0.1−2.0 M reduces the fade rate from ∼100%/day to only ∼0.4%/day in 2.0 M OH^-. Interestingly, the fade rate in 2.0 M OH^- is very close to the fade rate of 0.38%/day previously reported in 1.0 M OH^- when the electrochemical regeneration technique was implemented.[16] Clearly, raising the concentration of OH^- beyond 1.0 M can noticeably reduce the fade rate. We note that at higher OH^- concentrations, the

https://doi.org/10.1021/acsami.4c06073
ACS Appl. Mater. Interfaces 2024, 16, 52144−52152

Scheme 1. Disproportionation Reaction of $DHAQ^{4-}$[14,17]

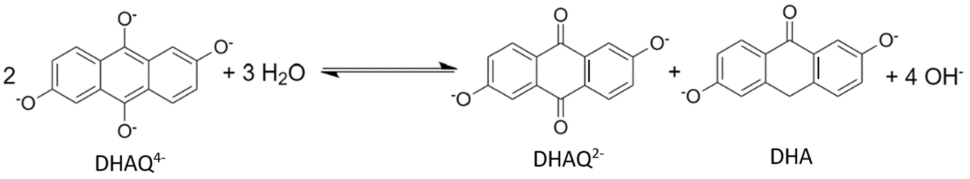

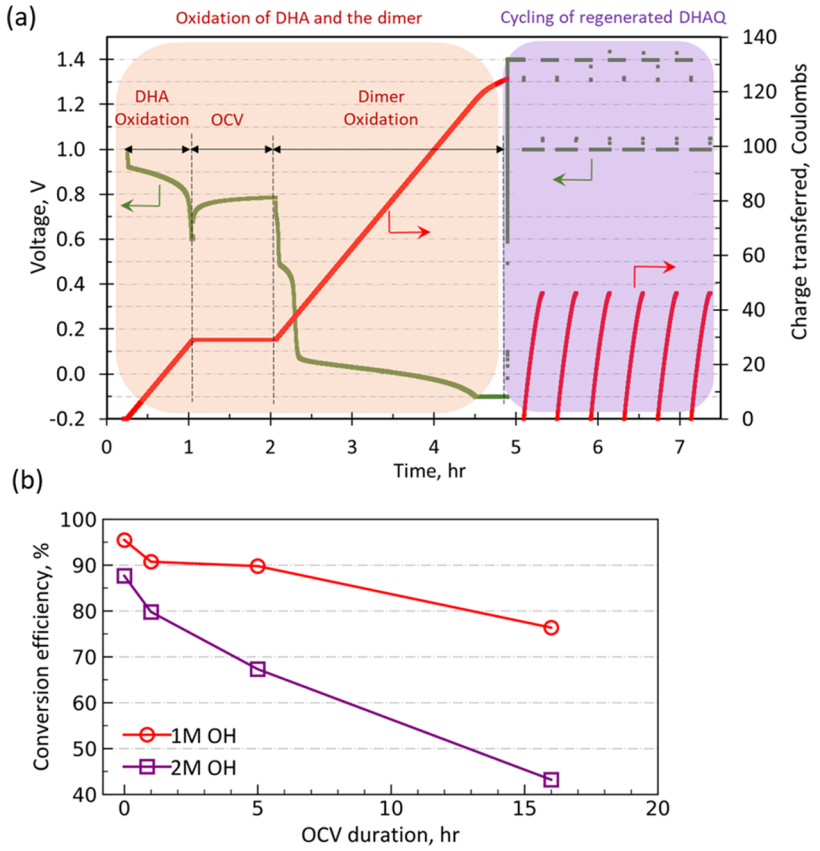

Figure 2. Conversion of DHA to DHAQ. (a) Time dependence of voltage and charge transferred in a DHA | ferro/ferricyanide full cell in 2 M OH^- (KOH). (b) Conversion efficiency vs OCV duration. Test conditions: negolyte contained 6.5 to 7.0 mL of 0.05 M DHA, and the posolyte comprised 120 mL of 0.04 M potassium ferrocyanide and 0.02 M potassium ferricyanide. DHA oxidation conditions: constant current density at 2 mA/cm^2 followed by potentiostatic hold at 0.6 V until a cutoff current density of 0.75 mA/cm^2 was reached. Dimer oxidation conditions: constant current density at 2 mA/cm^2 followed by potentiostatic hold at −0.1 V until a cutoff current density of 0.75 mA/cm^2 was reached. Cycling of the formed DHAQ: constant current density of 50 mA/cm^2 followed by a potentiostatic hold. The cutoff voltage for the charge and discharge steps were 1.4 and 1.0 V, respectively. Cutoff current densities for the charge and discharge steps were 2 mA/cm^2.

solubility of DHAQ decreases. Although the solubility[12] of DHAQ is >0.6 at 1.0 M KOH, it declines to around 0.2 at 2.0 M KOH.

The effect of the OH^- concentration on the fade rate can be understood by considering the disproportionation reaction of $DHAQ^{4-}$. As shown in Scheme 1, 4 mol of OH^- are formed when two moles of $DHAQ^{4-}$ disproportionate. At elevated OH^- concentration, the equilibrium shifts to the left, favoring $DHAQ^{4-}$ over the formation of DHA.

Electrochemical Regeneration. To achieve a low fade rate, the electrochemical regeneration technique was integrated into cell cycling in 2.0 M OH^-. Because the fade rate in 2.0 M OH^- is reasonably low (~0.4%/day), we hypothesized that, in combination with the effect of regeneration, the fade rate should be lowered dramatically. As shown and annotated in Figure S2, however, the regeneration in 2.0 M OH^- is noticeably less effective and unpredictable in contrast to the value of 90% previously reported for 1.0 M OH^-.[16] Interestingly, when the discharge cutoff voltage was raised to 0.95 V or higher, the recovery efficiency, defined as the fraction of the electroactive species lost since the previous regeneration step that is converted back into electroactive species during the regeneration step (eq S(2) in Section 1.1 in the SI), became repeatable and remained at 88%. The effectiveness of the regeneration step thus appears to be very sensitive to the cycling discharge cutoff voltage.

Stability of DHA and the Dimer. To understand the observations described above, we investigated how DHA, the disproportionation product of $DHAQ^{4-}$, is affected under various cycling conditions in the negolyte against a ferro/ferricyanide posolyte. We define the conversion efficiency as the fraction of DHA converted to DHAQ (eqs S(4)−S(6) described in Section 1.2 in the SI). Because the main decomposition product in a DHAQ | ferro/ferricyanide cell

https://doi.org/10.1021/acsami.4c06073
ACS Appl. Mater. Interfaces 2024, 16, 52144−52152

is DHA,[14] the conversion efficiency is expected to remain the primary determinant of the recovery efficiency. However, other decomposition mechanisms, the implications of which are not entirely discerned, may also contribute to the recovery efficiency.

In Figure 2a, we show the cell voltage vs time starting with 100% DHA at t = 0. DHA oxidation commences at approximately 0.2 h and ends at 1.0 h. Next, the cell is held at open circuit for the second hour, and then put through another negolyte oxidation step at a very low cell voltage (−0.1 V) for 2−5 h. Finally, the last 3 h are devoted to cycling with voltage and current cutoff values appropriate for DHAQ, to evaluate the discharge capacity attributable to the DHAQ formed from DHA. The amount of DHAQ, reckoned from the accessed discharge capacity, is compared to the theoretical amount that may possibly form from the initial DHA, and their ratio is reported in Figure 2b.

Examination of the voltage profile during the oxidation of DHA reveals that this compound turns into the DHA dimer at a quite high cell voltage, around 0.9 V. Thus, if the discharge cutoff voltage of a DHAQ | ferro/ferricyanide cell is set at or below this value, then DHA, which forms gradually due to the disproportionation of $DHAQ^{4-}$ (Scheme 1), may get electrochemically oxidized to the dimer even during regular cycling. Consequently, a mixture of DHA and a dimer exists in the negolyte well before the onset of a regeneration step. Thus, we hypothesized that the inefficiency of the regeneration procedures at discharge cutoff voltages of 0.9 V or lower in Figure S2 is related to the gradual decomposition of DHA, the dimer, or both, exacerbated at higher OH^- concentrations. The hypothesized decomposition reactions starting from DHA and the dimer are shown by red arrows and labeled as either (1) or (2) in Scheme 2 and are assumed to be homogeneous

Scheme 2. Reactions Considered in a DHAQ Negolyte[a14]

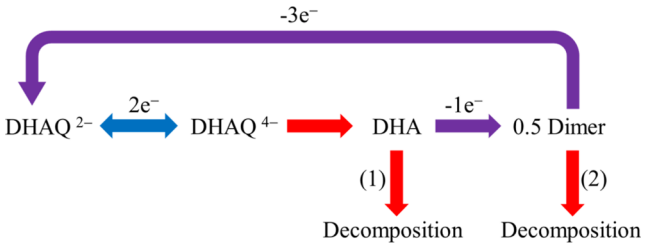

[a]Blue arrow: electrochemical reactions during regular cycling; red arrows: decomposition reactions; purple arrows: electrochemical reactions for the regeneration of DHAQ from DHA. Red arrows labeled as either (1) or (2) are decomposition reactions hypothesized in this work, and the rest are adapted from ref 14.

chemical reactions. Disproportionation reaction of $DHAQ^{4-}$ to DHA is also shown by a red arrow. Note that this scheme does not intend to show an exhaustive reaction pathway.

To test the hypothesis, experiments were performed using chemically synthesized DHA instead of analyzing the DHA that gradually accumulates through cycling of DHAQ. The latter process is very slow, especially in 2.0 M OH^- where the fade rate is only ∼0.4%/day (Figure 1). The same amount of DHAQ was generated by electrochemical oxidation of a freshly made DHA electrolyte and of an otherwise identical electrolyte that sat for more than 4 weeks under an inert nitrogen atmosphere. Note the amount of DHAQ was estimated from the discharge capacity measured during subsequent cycling with voltage and current cutoff values relevant to DHAQ (see Figure 2a, and eqs S(4)−S(6) in Section 1.2 in the SI). This observation indicates that DHA itself is chemically stable and does not undergo any chemical decomposition. Therefore, the red arrow labeled as (1) represents a reaction that either does not occur or occurs at a negligible rate.

To test the possibility of the chemical decomposition of the dimer, i.e., reaction (2) in Scheme 2, DHA is oxidized to the dimer, but the electrochemical oxidation of the dimer is delayed for a certain amount of time, referred to as "OCV duration", during which the cell is kept under OCV, to evaluate the extent of dimer decomposition under OCV conditions. Figure 2a shows a sample plot of voltage and charge transfer of a test with only 1 h of the OCV duration. Tests were performed with various OCV durations. The electrochemical oxidation of the remaining dimer is then initiated with a deep discharge.

As shown in Figure 2b, a longer duration of the OCV leads to less formation of DHAQ from the dimer. Although over 95% of DHA is converted to DHAQ with a zero OCV duration, the conversion efficiency drops to 76% with 16 h of OCV duration. This adverse effect is more pronounced at elevated OH^- concentration, where the conversion efficiency drops to 43% with 16 h of the OCV duration. This suggests that the dimer decomposes more rapidly with an increasing OH^- concentration. To minimize its decomposition, the dimer should be converted to DHAQ as soon as the dimer forms. Figure 2b also shows that even with zero OCV duration, the conversion of DHA to DHAQ is incomplete and lower in 2.0 M OH^- than in 1.0 M OH^-. This observation suggests that the decomposition of the dimer can be limited but not entirely prevented because of its fast decomposition rate. Note that we cannot exclude the possibility of other decomposition reactions that may occur during the oxidation of DHA. However, no decomposition products were observed using NMR. In Figure 2a, another electrochemical reaction takes place at around 0.45 V; however, the origin of the reaction is still unclear. Most likely, this reaction is related to the oxidation of species formed chemically during the OCV hold as the passed charge increases with longer OCV duration. As can be seen in Figures 2a and S3a, during the electrochemical oxidation at around 0.45 V, 10 and 170 coulombs were transferred when the OCV duration increased from 1 or 20 h, respectively.

In order to investigate side products that may form during the conversion of DHA to DHAQ, a DHA negolyte was oxidized, and species in the negolyte were tracked during the conversion via liquid chromatography−mass spectrometry (LC-MS). The results are presented in Figure S4 and indicate that the dimer is oxidized by homogeneous chemical reaction(s) even when it is left under OCV. In addition to the formation of DHAQ (m/z = 239.03), other previously unexplored species that have m/z = 461.07, 463.08, and 477.08 also grow. Based on Figure S4b, the subsequent electrochemical oxidation process enables the formation of DHAQ from the decomposed species. Nevertheless, the residual species (m/z = 463.08 and 479.08) imply that the regeneration process fails to convert all of the dimer to DHAQ; in other words, the DHA dimer is irreversibly decomposed to these species, leading to a permanent capacity loss.

Scheme 3 depicts proposed molecular structures with m/z values found by LC-MS analysis and the hypothesized DHA dimer chemical decomposition pathways. The high concentration of hydroxide ions facilitates the deprotonation of

https://doi.org/10.1021/acsami.4c06073
ACS Appl. Mater. Interfaces 2024, 16, 52144−52152

Scheme 3. Proposed Molecular Structures with m/z Values Found by LC−MS Analysis and the Hypothesized DHA Dimer Decomposition Pathways

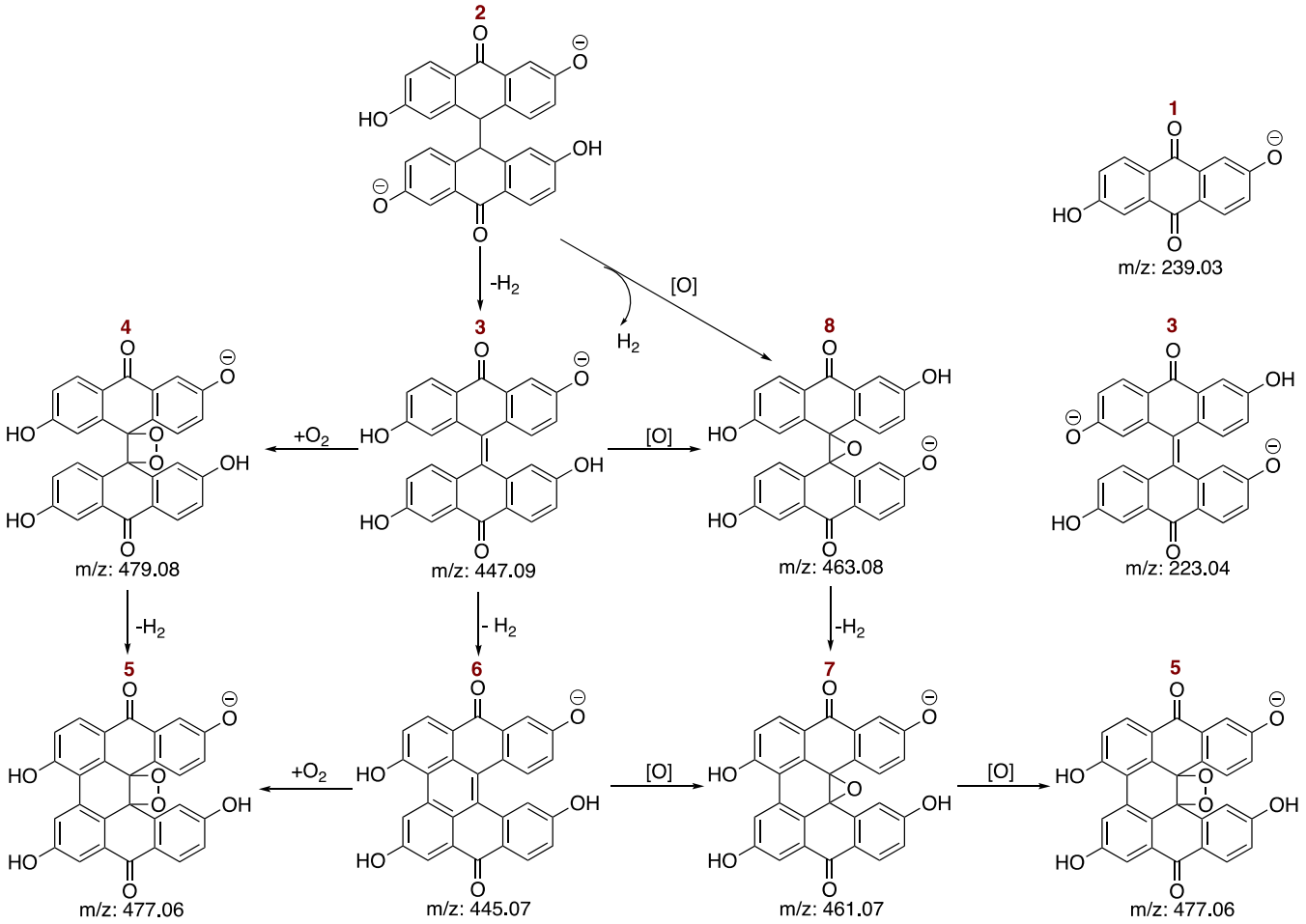

methine groups in $(DHA)_2$ (**2**), thus driving the electrochemical desaturation to produce **3**, which may be related to the voltage plateau starting at 0.4 V in Figure 2a. **3** can be oxygenated to form **4** and **8** particularly under the LC-MS condition where oxygen and high ionization energy were involved. The compounds **3**, **4**, and **8** can undergo dehydrogenative cyclization reactions to produce **6**, **5**, and **7**, respectively; corresponding m/z values have been detected from the LC−MS experiments. However, it is still unclear whether **4**−**8** were generated during the oxidation process in electrochemical flow cells then detected by the LC−MS experiments or produced under LC−MS experiment conditions in the presence of oxygen, as **4**−**8** were mainly observed in Samples 1 and 2. For Sample 3, the intensity of **1** increased, whereas the intensity of **4**, **7**, and **8** dropped. Nevertheless, we cannot rule out that **4**−**8** were further electrochemically oxidized to form polyfused aromatic species that became aqueous-insoluble and precipitated on electrodes or other cell parts and, thus, less likely to be detected through LC−MS experiments. Further mechanistic insight needs additional study. Note that the proposed new compounds **3**−**8** in Scheme 3 reflect the m/z values detected from our LC-MS experiments where oxygenation and dehydrogenation are plausible reaction pathways. Given that none of the compounds **3**−**8** have been detected and confirmed by NMR or other structural characterization techniques, it is possible that the detected m/z values come from other isomeric structures with identical chemical formulas, which are not shown in Scheme 3.

With the insights gained on the decomposition of dimer, we can now explain our earlier observation where lowering the discharge cutoff potential to 0.3 V adversely affects the DHAQ recovery efficiency (Figure S2). Conversion of DHA to DHAQ includes two electrochemical oxidation reactions, as depicted in Scheme 2: DHA → 0.5 Dimer and then 0.5 Dimer → DHAQ. Between these two, the first reaction proceeds at a higher cell voltage (e.g., a less positive oxidation potential for the negolyte) than the second: as shown in Figure 2a, the first and second reactions are initiated at cell voltages of about 0.9 and 0.0 V, respectively, and proceed to completion as the cell voltage is lowered further, increasing the driving force for the reactions. Lowering the cycling discharge cutoff voltage to 0.3 V not only oxidizes the $DHAQ^{4-}$ (reduced form of DHAQ) but also oxidizes any DHA formed during the disproportionation reaction to the dimer. Nevertheless, the cell voltage is not low enough to proceed to the oxidation of the dimer; this causes the accumulation of dimer, which is unstable, in the electrolyte. The dimer undergoes a decomposition reaction until the cell voltage is lowered enough during the deep-discharge step to oxidize the remaining dimer. The underlying reasons for the stability difference between DHA and the dimer need further investigation.

Therefore, we conclude that the cell discharge cutoff voltage should be set high enough (0.95 V or higher for the conditions

https://doi.org/10.1021/acsami.4c06073
ACS Appl. Mater. Interfaces 2024, 16, 52144−52152

tested in this study) to prevent the oxidation of DHA to the dimer. Otherwise, the dimer gradually forms from the partial oxidation of DHA and decomposes, and consequently, both the conversion efficiency and the recovery efficiency are diminished.

Regeneration Cutoff Voltage Effect. Another critical factor that may impact the effectiveness of regeneration is the cutoff voltage of the regeneration step itself. Figure 2a shows that the dimer oxidation is initiated at a cell voltage of around 0.0 V. However, it is crucial to determine the minimum cutoff voltage at which dimer oxidation completes, but the other species present in the negolyte remain unchanged. Unnecessarily lowering the regeneration cutoff voltage, which causes a higher oxidative potential for the negolyte, leads to the possibility of oxygen evolution reaction,[18] and also the oxidation of the carbonaceous electrode itself.[19] More importantly, very high oxidative voltages may also result in the decomposition of the electroactive species, DHAQ in our case. As presented in Figure S5, applying a very negative voltage (−0.4 V) to a DHAQ | Ferrocyanide cell led to the formation of side products in the negolyte not present in a pristine DHAQ electrolyte.

Figure 3a,b shows the dependency of the conversion efficiency on regeneration cutoff voltage and the highest

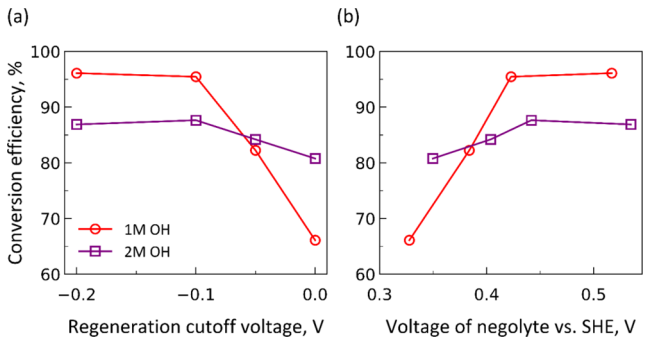

Figure 3. Conversion efficiency of DHA to DHAQ as a function of (a) cell regeneration cutoff voltage and (b) maximum oxidation voltage (vs SHE) that the negolyte experiences during the regeneration step. Test conditions: negolyte contained 6.5−7.0 mL of 0.05 M DHA and the posolyte comprised 120 mL of 0.04 M potassium ferrocyanide and 0.02 M potassium ferricyanide. DHA oxidation conditions: constant current density at 2 mA/cm^2 followed by potentiostatic hold until a cutoff current density of 0.75 mA/cm^2. Subsequent cycling of the formed DHAQ was performed under a constant current density at 50 mA/cm^2 followed by a potentiostatic hold. The cutoff voltage for the charge and discharge steps were 1.4 and 1.0 V, respectively. Cutoff current densities for the charge and discharge steps were 2 mA/cm^2.

potential that the negolyte experiences. The experiments were performed using chemically synthesized DHA instead of oxidizing the DHA that gradually forms through cycling of DHAQ. Not only does this approach shorten the length of experiments, but it also decreases the uncertainty in the results.

According to Figure 3a, the conversion of DHA to DHAQ is incomplete at a regeneration cutoff voltage of 0.0 V. Although a conversion efficiency of almost 80% is achieved in 2.0 M OH^-, the efficiency in 1.0 M OH^- is only 65% at the 0.0 V regeneration cutoff. Lowering the cutoff voltage to −0.1 V, i.e., reverse-polarizing the cell, raises the conversion efficiency. The dependence of the conversion efficiency on the cutoff voltage is more intense in 1.0 M OH^-. This figure corroborates the implication from Figure 2b that some amount of dimer decomposition is inevitable, and a conversion of 100% does not seem attainable. Figure 3a also shows that lowering the cell regeneration cutoff voltage below −0.1 V does not improve the conversion efficiency.

The cell voltage for the regeneration step should be adjusted accordingly when a posolyte with a different composition is used. Figure 3b shows the conversion efficiency vs the maximum potential the negolyte experiences at each regeneration cutoff voltage reported in Figure 3a. These values were measured with the help of a reference electrode (RE) as described in the SI (Figure S7). According to Figure 3b, the conversion efficiency approaches a maximum when the negolyte experiences an oxidation potential of around 0.45 V (vs SHE) beyond which the conversion efficiency remains essentially unchanged.

For the results reported in Figure 3, the electrochemical oxidations were performed under a constant current (CC) step followed by a constant-voltage (CV) step to exclude the impact of cell internal resistance changes on the extent of the reaction completion.[20] The CC step was usually set at a current density of 2 mA/cm^2 to force a slow oxidation reaction for both DHA and the dimer. To explore whether the oxidation rate affects the conversion efficiency, oxidation was performed an order of magnitude more rapidly at a current density of 20 mA/cm^2. With such a change, in 2.0 M OH^- and a cutoff voltage of −0.1 V, the conversion efficiency remained almost unchanged. However, at a cutoff voltage of −0.2 V, the conversion efficiency decreased to 84% at 20 mA/cm^2 from 89% at 2 mA/cm^2. Although this variation is quite small, such a decline may further confirm the adverse effect of a very low cutoff voltage on the conversion of DHA to DHAQ.

This observation, which seems consistent with the slight decline in the conversion shown in Figure 3 in 2 M OH^- at cutoff voltages lower than −0.1 V, may be explained as follows. Under slow DHA/dimer oxidation, most of the reaction occurs in the CC region at a voltage above the cutoff value; see, e.g., Figure 2a. At a faster DHA/dimer oxidation rate, however, the cell voltage quickly approaches the cutoff voltage. If the main electroactive species, DHAQ in this case, is unstable at very low cell voltages, as indicated by Figure S5, then more DHAQ may decompose when the cell spends longer at lower voltages during the faster oxidation rate. Although the cutoff voltage for the results shown in Figure S5 is −0.4 V, DHAQ may decompose to a lesser extent at the cutoff voltages explored in Figure 3. We interpret these results to mean that the rate of oxidation of DHA does not adversely affect the conversion efficiency as long as the cutoff voltage is not harmful to the main reactive species. This safe cutoff cell voltage appears to be closer to −0.1 V, i.e., a negolyte voltage of 0.45 V vs SHE. Thus, the conversion of DHA to DHAQ can be performed faster only if the cutoff voltage is chosen properly.

Period of Electrochemical Regeneration Events. It is crucial to determine how the period of performing the regeneration events impacts the recovery efficiency. Period is defined as the amount of time between the initiation of successive regeneration steps. We hypothesized that the effect of the period is linked to the DHA concentration accumulated in the electrolyte. To investigate this issue, two sets of experiments were performed.

For the first set, the conversion of DHA to DHAQ was measured at different initial concentrations of DHA. The oxidation of DHA and cycling of the formed DHAQ were

https://doi.org/10.1021/acsami.4c06073
ACS Appl. Mater. Interfaces 2024, 16, 52144−52152

performed under conditions similar to those described in Figure 3. In 2.0 M OH^-, when the DHA initial concentration is reduced from 50 to 2.5 mM, the conversion efficiency changes only from 88 to 85%. This change, however, is not significant because of the uncertainties involved in measuring transferred charges in the experiment. Therefore, within experimental error, the conversion efficiency appears to be essentially independent of the DHA concentration present in the electrolyte.

The second set of experiments was performed using cells initially containing DHAQ in which DHA formed and accumulated gradually during cycling from the $DHAQ^{4-}$ disproportionation. In this set of tests, the period between regeneration events was varied. The recovery efficiencies are reported in Figure 4.

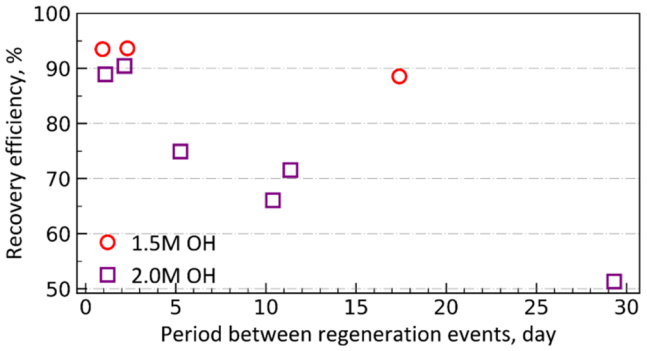

Figure 4. Recovery efficiency vs period between regeneration events. Test conditions: negolyte comprised 7.0 mL (10 mL for the test in 1.5 M OH^-) of 0.1 M DHAQ and the posolyte comprised 120 mL of 0.06 M potassium ferrocyanide and 0.03 M potassium ferricyanide. Cell cycling was performed under a constant current density of 50 mA/cm^2 followed by a potentiostatic hold. The cutoff voltage for the charge and discharge steps were 1.4 and 1.0 V, respectively. Cutoff current densities for the charge and discharge steps were 2 mA/cm^2. Regeneration steps were performed under a constant current density of 10 mA/cm^2 followed by a potentiostatic hold at −0.15 V until a cutoff current density of 0.75 mA/cm^2 was reached.

As shown in Figure 4, the recovery efficiency declines significantly when the period between regeneration events increases. For these experiments, cells were cycled with a discharge cutoff voltage of 0.95 V or higher, which is high enough to prevent the formation of the unstable dimer until the regeneration step is initiated. In 2.0 M OH^-, although the recovery efficiency is over 88% when the regeneration step is performed every 1 or 2 days, it drops significantly with increasing period. The same trend is observed for 1.5 M OH^-; however, the extent of the decline is noticeably lower.

Thus, Figure 4 clearly shows that regeneration should be performed frequently to retain a high recovery efficiency over the long term. This may, however, increase the risk of the cell. The risk is that the oxygen evolution reaction (OER) may also proceed at the negative electrode during the regeneration step. Given that the OER consumes OH^-, the pH of the negolyte gradually declines, and consequently, the fade rate of the cell is accelerated (Figure 1b). Nevertheless, if the regeneration cutoff voltage is chosen properly (Figure 3), then the extent of the OER can be reduced. Alternatively, after the regeneration step, oxygen (air) can be introduced into the negolyte to counteract the imbalance. This approach, however, requires measuring the pH of both the posolyte and negolyte to prevent overexposure of oxygen.

Electrochemical Regeneration Plus SOC Restriction. After realization of the importance of the operating conditions as discussed above, experiments were designed to determine the minimum achievable fade rate for a DHAQ | ferrocyanide/ferricyanide cell. Cycling tests were performed at OH^- concentrations of 1.0, 1.5, and 2.0 M. SOC restriction and regeneration techniques were integrated into cell cycling, and operating conditions, such as cutoff voltage of the discharge and regeneration steps, were chosen properly to obtain the lowest fade rate at each of the OH^- concentrations. The results are presented in Figure 5.

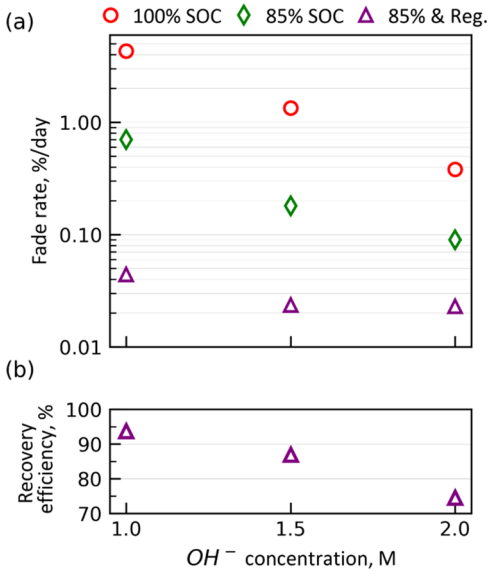

Figure 5. (a) Fade rate vs KOH concentration under the following conditions: 100% cycling, 0−85% SOC cycling, and 0−85% SOC cycling combined with regeneration. (b) Recovery efficiency vs KOH concentration for the cycling case when 0−85% SOC and the regeneration step are combined. The tests were run for an extended amount of time; the sequence of 0−85% SOC cycling followed by a regeneration step was repeated at least 6 times. Recovery efficiency and fade rates are the averages over the entire test (see SI Section 1.1, Figure S1, and eqs S(1)−S(3) for more details). Test conditions: negolyte comprised 7.0 mL (or 10 mL for the test in 1.5 M KOH) of 0.1 M DHAQ and the posolyte comprised 120 mL of 0.06 M potassium ferrocyanide and 0.03 M potassium ferricyanide. Cell cycling was performed under a constant current density of 50 mA/cm^2, followed by a potentiostatic hold. The cutoff voltage for the charge and discharge steps were 1.4 and 1.0 V, respectively. Cutoff current densities for the charge and discharge steps were 2 and 1 mA/cm^2, respectively. For the 0−85% SOC restriction step, charging capacity was controlled not to exceed 85% of the total capacity of the cell. Regeneration steps were performed under a constant current density at 10 mA/cm^2 followed by a potentiostatic hold at −0.15 V until a cutoff current density of 0.75 mA/cm^2 was reached.

Figure 5a shows the fade rate versus OH^- concentration under different cycling conditions including 100, 0−85% SOC restriction, and 0−85% SOC restriction combined with a regeneration step; the values at 100% cycling are copied from Figure 1 for comparison purposes. The impact of SOC restriction on the fade rate of a DHAQ flow cell was previously reported in 1 M OH^-.[14] However, Figure 5a shows how a combination of SOC restriction cycling and OH^- concen-

https://doi.org/10.1021/acsami.4c06073
ACS Appl. Mater. Interfaces 2024, 16, 52144−52152

tration affects the fade rate. Under 0−85% SOC cycling conditions, as the OH^- concentration increases to 2.0 M, the fade rate decreases to 0.09%/day. Thus, with a combination of 85% SOC restriction and OH^- concentration, a fade rate of 0.09%/day is achievable that is ∼8 and ∼45 times lower than the fade rate in 1 M OH^- with and without employing 0−85% SOC restriction, respectively. This observation confirms that increasing the OH^- concentration beyond 1.0 M significantly reduces the fade rate, even when the SOC restriction technique is utilized.

Figure 5a also shows the fade rate for the case when 0−85% SOC restriction and regeneration are both integrated into the cell cycling. The measured fade rate in 1.0 M OH^- is around 0.05%/day (18.3%/year) but it decreases to 0.02%/day (7.3%/year) in 1.5 M OH^-. Nonetheless, the fade rate remains unchanged when the OH^- concentration is further increased to 2.0 M. Therefore, there is no benefit to the fade rate by increasing the OH^- concentration beyond 1.5 M when both SOC restriction and regeneration are implemented. This observation is related to a lower recovery efficiency. As shown in Figure 5b, the recovery efficiency decreases to 74% in 2.0 M OH^-. Although the lowest fade rate is obtained in 2 M OH^- under both 100% cycling and 0−85% cycling conditions, the fade rate in the presence of regeneration is not lowered because the recovery efficiency is the lowest in 2.0 M OH^-. It should be noted that part of the fade rate reported in Figure 5 may be due to the permeation of the electroactive species, DHAQ in this case, through the membrane, meaning that the capacity fade rates reported here represent upper limits of the molecular decomposition rate. A calculation reported in the SI (eq S(7) described in Section 1.3) yields an estimate of 0.19%/day.

Due to performing the regeneration step, a loss in energy efficiency is anticipated. Nevertheless, this loss is negligible and remains lower than 0.5% as shown in Figure S6. Therefore, the energy cost of regeneration is not a critical factor in determining the period between regeneration events.

The minimum fade rate of 0.02%/day demonstrated in this study is the lowest ever reported for a DHAQ | ferrocyanide/ferricyanide flow cell. At such *a* low fade rate, given its low estimated cost of manufacture, DHAQ may now become *a* viable negotiator for some energy storage applications.

CONCLUSIONS

In this study, we explore the dependency of the capacity fade rate of a flow battery utilizing 2,6-dihydroxyanthraquinone (DHAQ) as the negolyte on conditions including hydroxide concentration, state of charge (SOC) limits, cutoff voltage of the discharge step, cutoff voltage for electrochemical regeneration by oxidation of decomposition compounds back to active species, and periodicity of performing electrochemical regeneration.

Our experiments confirm that increasing the OH^- concentrations from 1.0 to 1.5 and 2.0 M decreases the fade rate from 4.3%/day to 1.34 and 0.38%/day, respectively. Under 0−85% SOC restriction conditions, the fade rate at those OH^- concentrations reaches 0.7, 0.18, and 0.09%/day, respectively. Clearly, combining 0−85% SOC cycling with higher OH^- concentrations greatly decreases the fade rate. Additionally, with the effect of the regeneration technique, the fade rate is observed to be around 0.05 and 0.02%/day in 1.0 and 1.5 M OH^-, respectively. The fade rate in 2.0 M OH^- is also 0.02%/day, which is not lower than that in 1.5 M OH^- because of the lower recovery efficiency. The recovery efficiency drops from 94 to 87% and to 74% as the OH^- concentration increases from 1.0 to 1.5 and 2.0 M.

The recovery efficiency also depends on the periodicity of performing the regeneration technique. To achieve higher recovery efficiencies, it seems essential to perform the regeneration step very frequently. Given a higher fade rate in 1 M OH^-, a more frequent regeneration step is needed. The associated loss in energy efficiency remains lower than 0.5%.

Employing the recommendations and choosing proper cycling conditions for DHAQ enable us to achieve a fade rate as low as 0.02%/day. This fade rate is 18 times lower than the lowest rate reported previously of 0.38%/day and over 200 times lower than the value under standard cycling conditions of 4.5%/day. In our interpretation of the results, the first decomposition product, 2,6-dihydroxyanthrone, is stable, but after electro-oxidative dimerization, the anthrone dimer decomposes; the underlying reason for this stability difference could benefit from deeper investigation. We identify conditions for which there is little time after dimerization until the dimer is rapidly reoxidized electrochemically to form 2,6-dihydroxyanthraquinone. The findings and their mechanistic interpretation are expected to extend the lifetime and enhance the effectiveness of in situ electrochemical regeneration for other electroactive species with finite lifetimes. Here we list recommendations for controlling the fade rate of anthraquinone-based flow cells with a finite lifetime.

- Increasing the OH^- concentration above 1.0 M significantly reduces the fade rate.
- The discharge cutoff voltage should be adjusted such that the formation of DHA dimer, which is unstable chemically, is eliminated until when the regeneration step is initiated.
- Combining SOC restriction and regeneration techniques is very effective in further reducing the fade rate.
- Choosing a proper cutoff voltage for the regeneration step is critical to maximize recovery efficiency while preventing the decomposition of electroactive species.
- The period between the start of successive regeneration events is another important factor affecting the recovery efficiency. Because the energy cost of regeneration is quite negligible, a low period between regeneration events is recommended.

ASSOCIATED CONTENT

Supporting Information

The Supporting Information is available free of charge at https://pubs.acs.org/doi/10.1021/acsami.4c06073.

Definitions of terms and procedure for SoC (state of charge) restriction tests; cell cycling; LC-MS and ^1H NMR tests and discussion on the decomposition; energy cost analysis of the electrochemical regeneration; materials and methods; and image of reference electrode installed in the cell (PDF)

AUTHOR INFORMATION

Corresponding Author

Michael J. Aziz − *John A. Paulson School of Engineering and Applied Sciences, Harvard University, Cambridge, Massachusetts 02138, United States;* orcid.org/0000-0001-9657-9456; Email: maziz@harvard.edu

https://doi.org/10.1021/acsami.4c06073
ACS Appl. Mater. Interfaces 2024, 16, 52144−52152

Authors

Meisam Bahari − *John A. Paulson School of Engineering and Applied Sciences, Harvard University, Cambridge, Massachusetts 02138, United States;* Present Address: Quino Energy, Inc., San Leandro, California 94577, United States; orcid.org/0000-0002-5800-3349

Yan Jing − *Department of Chemistry and Chemical Biology, Harvard University, Cambridge, Massachusetts 02138, United States;* Present Address: Department of Materials Science and Engineering, National University of Singapore, 117575 Singapore

Shijian Jin − *John A. Paulson School of Engineering and Applied Sciences, Harvard University, Cambridge, Massachusetts 02138, United States*

Marc-Antoni Goulet − *John A. Paulson School of Engineering and Applied Sciences, Harvard University, Cambridge, Massachusetts 02138, United States;* Present Address: Department of Chemical and Materials Engineering, Concordia University, Montreal, Quebec, H4B 1R6 Canada; orcid.org/0000-0002-9146-6759

Tatsuhiro Tsukamoto − *Department of Chemistry and Chemical Biology, Harvard University, Cambridge, Massachusetts 02138, United States*

Roy G. Gordon − *Department of Chemistry and Chemical Biology, Harvard University, Cambridge, Massachusetts 02138, United States;* orcid.org/0000-0001-5980-268X

Complete contact information is available at: https://pubs.acs.org/10.1021/acsami.4c06073

Author Contributions

M.B. developed the methods, designed the experiments, and conducted cell tests, electrochemical experiments, and analysis. Y.J. and S.J. performed the chemical characterization tests. Y.J., S.J., and T.T. proposed the decomposition mechanism. M-A.G. contributed to the experimental design and methodologies. R.G.G. supervised the chemical characterization. M.J.A. supervised the project. M.B., Y.J., and M.J.A. drafted the manuscript. All authors edited the manuscript.

Notes

The authors declare the following competing financial interest(s): Meisam Bahari, Marc-Antoni Goulet, Michael J Aziz, and Roy G Gordon have ownership stakes in Quino Energy, Inc., which may profit from the results reported in this study.

■ ACKNOWLEDGMENTS

The research was supported by US DOE award no. DE-AC05-76RL01830 through PNNL subcontract no. 654799 and by a grant from MassVentures. The funders had no role in study design, data collection and analysis, decision to publish, or preparation of the manuscript. The authors thank Eric M. Fell, Eliza K. Spear, Taobo Wang, and Dr. Kiana Amini for useful discussions.

■ REFERENCES

(1) Rugolo, J.; Aziz, M. J. Electricity Storage for Intermittent Renewable Sources. *Energy Environ. Sci.* **2012**, *5* (5), 7151−7160.

(2) Kittner, N.; Lill, F.; Kammen, D. M. Energy Storage Deployment and Innovation for the Clean Energy Transition. *Nat. Energy* **2017**, *2* (9), No. 17125.

(3) Skyllas-Kazacos, M.; Chakrabarti, M. H.; Hajimolana, S. A.; Mjalli, F. S.; Saleem, M. Progress in Flow Battery Research and Development. *J. Electrochem. Soc.* **2011**, *158* (8), R55−R79.

(4) Bahari, M.; Watt, G. D.; Harb, J. N. An Asymmetric Viologen-Based Negolyte with a Low Redox Potential for Neutral Aqueous Redox Flow Batteries. *J. Electrochem. Soc.* **2021**, *168* (9), No. 090525.

(5) Beh, E. S.; De Porcellinis, D.; Gracia, R. L.; Xia, K. T.; Gordon, R. G.; Aziz, M. J. A Neutral Ph Aqueous Organic-Organometallic Redox Flow Battery with Extremely High Capacity Retention. *Acs Energy Lett.* **2017**, *2* (3), 639−644.

(6) Ji, Y.; Goulet, M. A.; Pollack, D. A.; Kwabi, D. G.; Jin, S.; Porcellinis, D.; Kerr, E. F.; Gordon, R. G.; Aziz, M. J. A Phosphonate-Functionalized Quinone Redox Flow Battery at near-Neutral Ph with Record Capacity Retention Rate. *Adv. Energy Mater.* **2019**, *9* (12), No. 1900039.

(7) Jin, S.; Fell, E. M.; Vina-Lopez, L.; Jing, Y.; Michalak, P. W.; Gordon, R. G.; Aziz, M. J. Near Neutral Ph Redox Flow Battery with Low Permeability and Long-Lifetime Phosphonated Viologen Active Species. *Adv. Energy Mater.* **2020**, *10* (20), No. 2000100.

(8) Huskinson, B. T.; Marshak, M. P.; Suh, C.; Er, S.; Gerhardt, M. R.; Galvin, C. J.; Chen, X.; Aspuru-Guzik, A.; Gordon, R. G.; Aziz, M. J. A Metal-Free Organic-Inorganic Aqueous Flow Battery. *Nature* **2014**, *505* (7482), 195−198.

(9) Jing, Y.; Fell, E. M.; Wu, M.; Jin, S.; Ji, Y.; Pollack, D. A.; Tang, Z.; Ding, D.; Bahari, M.; Goulet, M.-A.; et al. Anthraquinone Flow Battery Reactants with Nonhydrolyzable Water-Solubilizing Chains Introduced Via a Generic Cross-Coupling Method. *Acs Energy Lett.* **2022**, *7* (1), 226−235.

(10) Wu, M.; Bahari, M.; Fell, E.; Gordon, R. G.; Aziz, M. J. High-Performance Anthraquinone with Potentially Low Cost for Aqueous Redox Flow Batteries. *J. Mater. Chem. A* **2021**, *9*, 26709−26716.

(11) Wu, M.; Bahari, M.; Jing, Y.; Amini, K.; Fell, E. M.; George, T. Y.; Gordon, R. G.; Aziz, M. J. Highly Stable Low Redox Potential Quinone for Aqueous Flow Batteries. *Batteries Supercaps* **2022**, *5*, No. e202200009.

(12) Lin, K.; Chen, Q.; Gerhardt, M. R.; Tong, L.; Kim, S. B.; Eisenach, L.; Valle, A. W.; Hardee, D.; Gordon, R. G.; Aziz, M. J.; Marshak, M. P. Alkaline Quinone Flow Battery. *Science* **2015**, *349* (6255), 1529−1532.

(13) Gregory, T. D.; Perry, M. L.; Albertus, P. Cost and Price Projections of Synthetic Active Materials for Redox Flow Batteries. *J. Power Sources* **2021**, *499*, No. 229965.

(14) Goulet, M. A.; Tong, L.; Pollack, D. A.; Tabor, D. P.; Odom, S. A.; Aspuru-Guzik, A.; Kwan, E. E.; Gordon, R. G.; Aziz, M. J. Extending the Lifetime of Organic Flow Batteries Via Redox State Management. *J. Am. Chem. Soc.* **2019**, *141* (20), 8014−8019.

(15) Zhao, E. W.; Liu, T.; Jonsson, E.; Lee, J.; Temprano, I.; Jethwa, R. B.; Wang, A.; Smith, H.; Carretero-Gonzalez, J.; Song, Q.; Grey, C. P. In Situ Nmr Metrology Reveals Reaction Mechanisms in Redox Flow Batteries. *Nature* **2020**, *579*, 224−228.

(16) Jing, Y.; Zhao, E. W.; Goulet, M. A.; Bahari, M.; Fell, E. M.; Jin, S.; Davoodi, A.; Jonsson, E.; Wu, M.; Grey, C. P.; et al. In Situ Electrochemical Recomposition of Decomposed Redox-Active Species in Aqueous Organic Flow Batteries. *Nat. Chem.* **2022**, *14* (10), 1103−1109.

(17) Wu, M.; Jing, Y.; Wong, A. A.; Fell, E. M.; Jin, S.; Tang, Z.; Gordon, R. G.; Aziz, M. J. Extremely Stable Anthraquinone Negolytes Synthesized from Common Precursors. *Chem* **2020**, *6*, 1432−1442.

(18) Dizaji, M. T.; Li, W. Higher Voltage Redox Flow Batteries with Hybrid Acid and Base Electrolytes. *Eng. Sci.* **2020**, *11*, 54−65.

(19) Möller, S.; Barwe, S.; Masa, J.; Wintrich, D.; Seisel, S.; Baltruschat, H.; Schuhmann, W. Online Monitoring of Electrochemical Carbon Corrosion in Alkaline Electrolytes by Differential Electrochemical Mass Spectrometry. *Angew. Chem., Int. Ed.* **2020**, *59* (4), 1585−1589.

(20) Goulet, M.-A.; Aziz, M. J. Flow Battery Molecular Reactant Stability Determined by Symmetric Cell Cycling Methods. *J. Electrochem. Soc.* **2018**, *165* (7), A1466−A1477.

Supporting Information

200-fold Lifetime Extension of 2,6- dihydroxyanthraquinone Electrolyte during Flow Battery Operation

Meisam Bahari [1,†], Yan Jing [2,‡], Shijian Jin [1], Marc-Antoni Goulet [1,ζ], Tatsuhiro Tsukamoto [2], Roy G Gordon [2], Michael J Aziz [1,]*

[1]John A. Paulson School of Engineering and Applied Sciences, Harvard University, Cambridge, MA, 02138 USA

[2] Department of Chemistry and Chemical Biology, Harvard University, Cambridge, MA, 02138 USA

[†] Present address: Quino Energy, Inc., San Leandro, CA, 94577 USA

[‡] Present address: Department of Materials Science and Engineering, National University of Singapore, 117575 Singapore

ζ Present address: Department of Chemical and Materials Engineering, Concordia University, Montreal, Quebec, H4B 1R6 Canada

Table of Contents

Section 1: Definitions

Section 1.1: SOC restriction test, regeneration technique, and fade rate estimation:

Fade rates for cell cycling conditions when no SOC restriction or regeneration technique are employed, are the slope of the line of best fit when the natural logarithm of capacity vs. time is plotted.

Cell cycling may consist of a procedure that involves an SOC restriction (for instance, 0-85% SOC) followed by regeneration step as presented in Figure 5. For these tests, the cell cycling procedure consists of the following steps.

a) cycling at 0-100% SOC for a few cycles to measure the initial capacity,

b) cycling at 0-85% SOC for the desired duration,

c) cycling at 0-100% SOC for a few cycles to measure the remaining capacity.

d) performing a recovery step,

e) cycling at 100% SOC for a few cycles to measure the regenerated capacity.

f) returning to step (b) for a few times (at least 6 times for the tests the result of which are presented in Figure 5).

Figure S1 shows an example of the capacity of a cell when 0-85% SOC restriction and regeneration techniques are both integrated into the cell cycling.

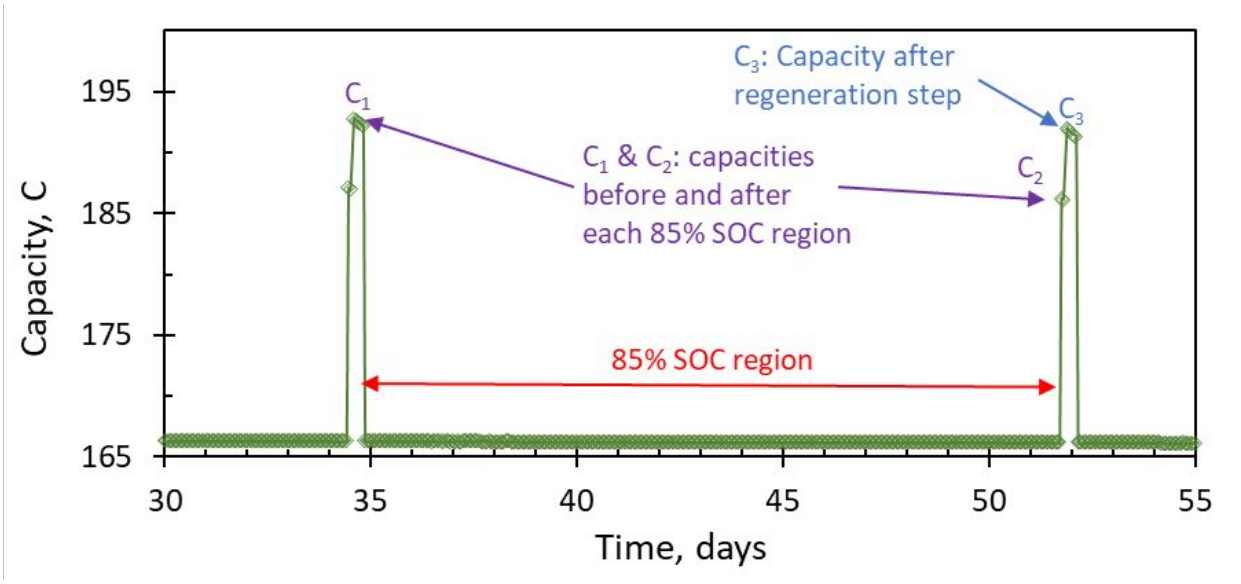

Figure S1. An example of capacity of a cell when 0-85% SOC restriction and regeneration techniques are integrated into the cell cycling. 85% SOC is determined based on the C_1 capacity.

The 0-85% SOC part (step b) is the main part of the test and lasts the longest compared to the rest of the procedure. The 100% SOC cycles (steps c and e) are performed to measure the remaining capacity before or after each regeneration step. 85% SOC is determined based on the C_1 capacity measured before starting a new 0-85% SOC cycling step. The duration of the 0-85% SOC cycling region in each repetition is estimated to last such that a total fade of at least 2.5% in capacity is measured to ensure a low uncertainty in the analysis. For instance, since the fade rate at 0-85% SOC and 1.5 M OH^- is estimated to be 0.2%/day, each step (b) is set to last two weeks (1-exp (14 days x 0.2%/day) =2.8%) or more. For the test at 1 M OH^-, each Step (b) lasts only one week over which the total fade in capacity is enough (1-exp (7 days x 0.7%/day) =4.8%). Each Step (b) for the test at 2 M OH^- lasts almost a month because the fade rate under 0-85% SOC is <0.09%/day.

Continuing each Step (b) at 2 M OH^- even longer than a month drops the uncertainty of the results more. However, limited resources prevented us from doing so given that 6 (or more) repetitions were planned for the tests. The test at 2 M OH^- continued for a total of more than eight months.

For the tests when SOC restriction and/or regeneration are integrated into cell cycling, fade rate for each of the SOC restriction repetitions is calculated as following:

$$\text{Fade rate} = \frac{\ln(\frac{C_2}{C_1})}{Time\ difference} \quad \text{S(1)}$$

where C_1 is the capacity of the cell before starting a new SOC restriction step. C_2 is the remaining capacity of the cell once a SOC restriction segment is complete.

Recovery efficiency of each regeneration event is defined as the fraction of the lost electroactive species converted back into electroactive species during the regeneration step and is calculated as:

$$\text{Recovery efficiency} = \frac{C_3 - C_2}{C_1 - C_2} \text{ x } 100\% \quad \text{S(2)}$$

C_3 is capacity once a regeneration step is complete (capacity measured in Step-e). The recovery efficiency for the entire test is the arithmetic average of the recovery efficiencies estimated separately for each of the regeneration events. Fade rate for the entire test is determined as:

$$\text{Fade rate} = \frac{\ln(\frac{C_{final}}{C_{initial}})}{Time\ difference} \quad \text{S(3)}$$

where $C_{initial}$ and C_{final} are the initial capacity of the cell at time zero and the remaining capacity once the final regeneration event is completed, respectively.

Section 1.2: Conversion of DHA to DHAQ:

Conversion efficiency is the fraction of DHA converted to DHAQ and is calculated by comparing the actual amount of DHAQ reckoned from the discharge capacity once the conversion process concludes, to the theoretical maximum amount that may possibly form from the initial DHA.

$$\text{Conversion efficiency} = \frac{actual\ moles\ of\ DHAQ}{theoretical\ maximum\ moles\ of\ DHAQ} \times 100\% \qquad \text{S(4)}$$

The actual moles of DHAQ is estimated using the following equation.

$$\text{Actual moles of DHAQ} = \frac{discharge\ capacity\ in\ coloumbs}{n \times F} \qquad \text{S(5)}$$

Where n is equal to 2 (the number of electrons transferred during charging/discharging DHAQ) and F is the Faraday's constant. Theoretical maximum moles of DHAQ is equal to the initial number of moles of DHA. Therefore, the conversion efficiency can be expressed as:

$$\text{Conversion efficiency} = \frac{\frac{discharge\ capacity\ in\ coloumbs}{n \times F}}{Initial\ moles\ of\ DHA} \times 100\% \qquad \text{S(6)}$$

Section 1.3: Permeability calculation for DHAQ:

Permeability of DHAQ through Nafion 115, which is very similar to Nafion 117 membrane used in this study, has been reported to be 9.9 x 10^{-4} cm^2/sec [1]. Solving the following equation which models crossover by diffusion based on Fick's Law [2],

$$\frac{dC}{dt} = -S\frac{P}{l}C \qquad \text{S(7)}$$

gives the fade rate due to permeation. In this equation, S is the ratio of the membrane area to the volume of the capacity limiting electrolyte, P is permeability, l is thickness of the membrane, t is time, and C is the concentration of the electroactive species. Under the conditions explored in this study, a fade rate of 0.019%/day is estimated solely due to the permeation through the membrane.

Section 2: Cycling at Various Discharge and Regeneration Cutoff Voltages

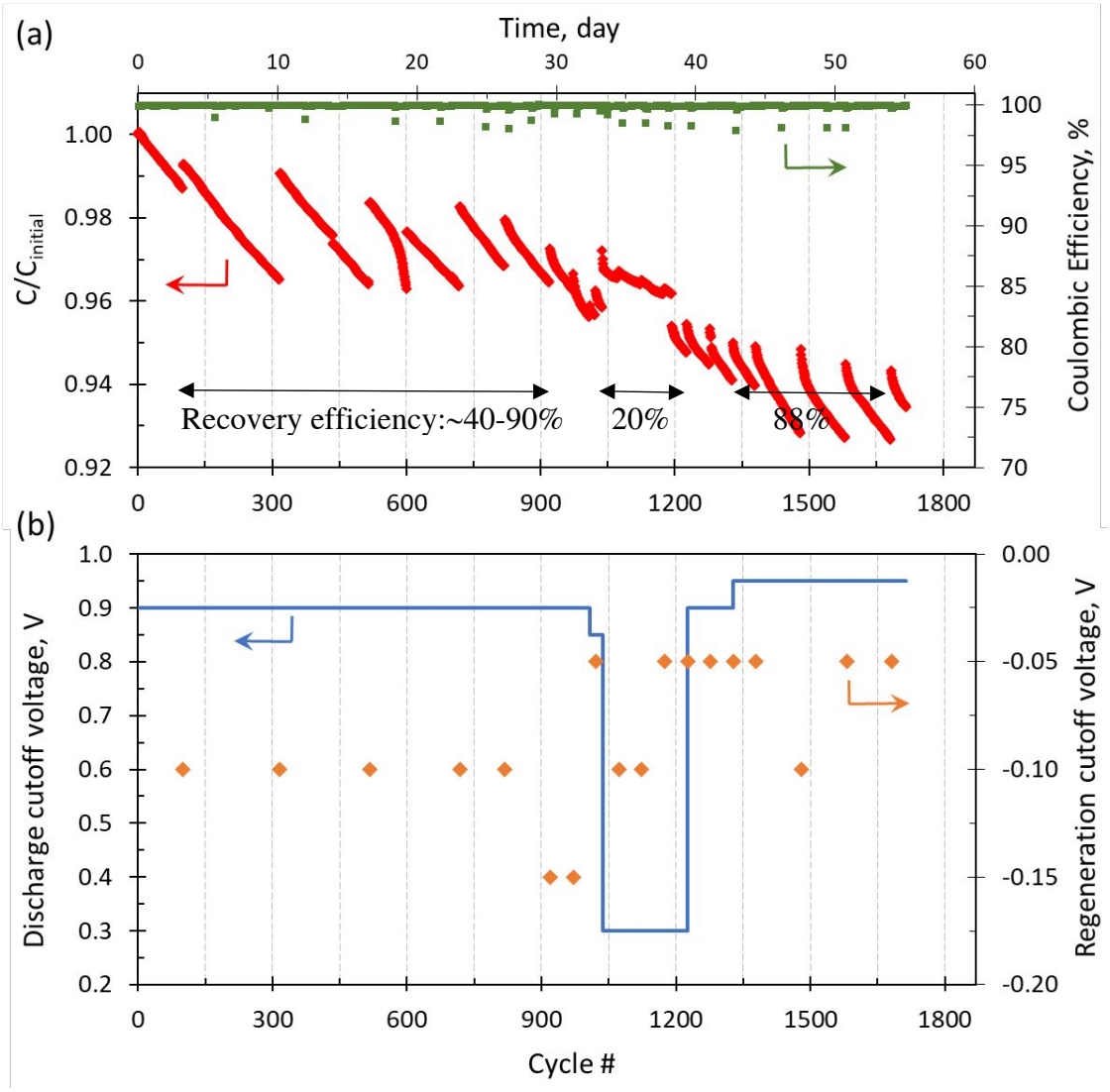

Figure S2. (a) Discharge capacity normalized by the initial discharge capacity and coulombic efficiency vs. time (or cycle number) in 2 M OH^-. Jumps in the normalized capacity are due to the regeneration steps performed. Recovery efficiencies are annotated on the plot. (b) cutoff voltage of the discharge and regeneration steps. Test conditions: negolyte contained 5.5 ml of 0.1 M DHAQ, and the posolyte consisted of 30 ml of 0.06 M potassium ferrocyanide and 0.03 M potassium ferricyanide. Both the posolyte and negolyte were in 2M OH^- concentration. Cycling

was performed under constant current density at 50 mA/cm^2 followed by potentiostatic hold. Cutoff voltage for the charge step was always 1.4V. Cutoff current densities for the charge and discharge steps were 2 and 1 mA/cm^2, respectively. The regeneration step was performed under a constant current density of 2 mA/cm^2 followed by a potentiostatic hold until a cutoff current density of 0.75 mA/cm^2 was reached.

Figure S2a shows the discharge capacity normalized by the initial discharge capacity of a cell in 2.0 M OH^-. For this test, the regeneration technique was integrated into the cell cycling. Cell cycling consisted of a procedure where the cell was charged/discharged for one to five days and then it underwent a regeneration step. Cycling of the cell was performed at a constant current density followed by a charge cutoff voltage of 1.4V and a discharge cutoff voltage that was varied from 0.95 V to 0.3 V. During the occasional regeneration step, a negative voltage was applied to the cell. The negative voltages for the regeneration steps were -0.05, -0.1, or -0.15 V. Figure S2b shows the cutoff voltages of the discharge and regeneration steps. The sudden jumps in capacity in Figure S2a show when the regeneration steps were performed. As annotated on Figure S2a, even when the discharge cutoff voltage was kept the same at 0.9 V, the recovery efficiency varied unpredictably in the range of 40% to 90%. Lowering the discharge cutoff voltage to 0.3 V decreased the recovery efficiency even further, to only 20%. When the discharge cutoff voltage was raised to 0.95 V or higher, the recovery efficiency became repeatable and remained at 88%.

The effectiveness of the regeneration step thus appears to be very sensitive to the cycling discharge cutoff voltage as discussed in detail in the main text.

Section 3: LC-MS Tracking of DHA Conversion to DHAQ

Figure S3a shows time-dependence of cell voltage and current during the conversion of DHA to DHAQ in in a DHA | ferro/ferricyanide cell. A series of electrochemical reactions were performed starting with the oxidation of DHA to the dimer from day 0.05 to 0.1, then a long OCV step until day 1 followed by electrochemical oxidation at a lower cell voltage until day 1.4. Next, the cell was cycled a few times to measure the amount of DHAQ formed during the process (the cycling part is not shown in this figure). In addition to the electrochemical steps performed, chemical reactions may possibly occur as depicted by blue arrows on Figure S3b, and lead to side products.

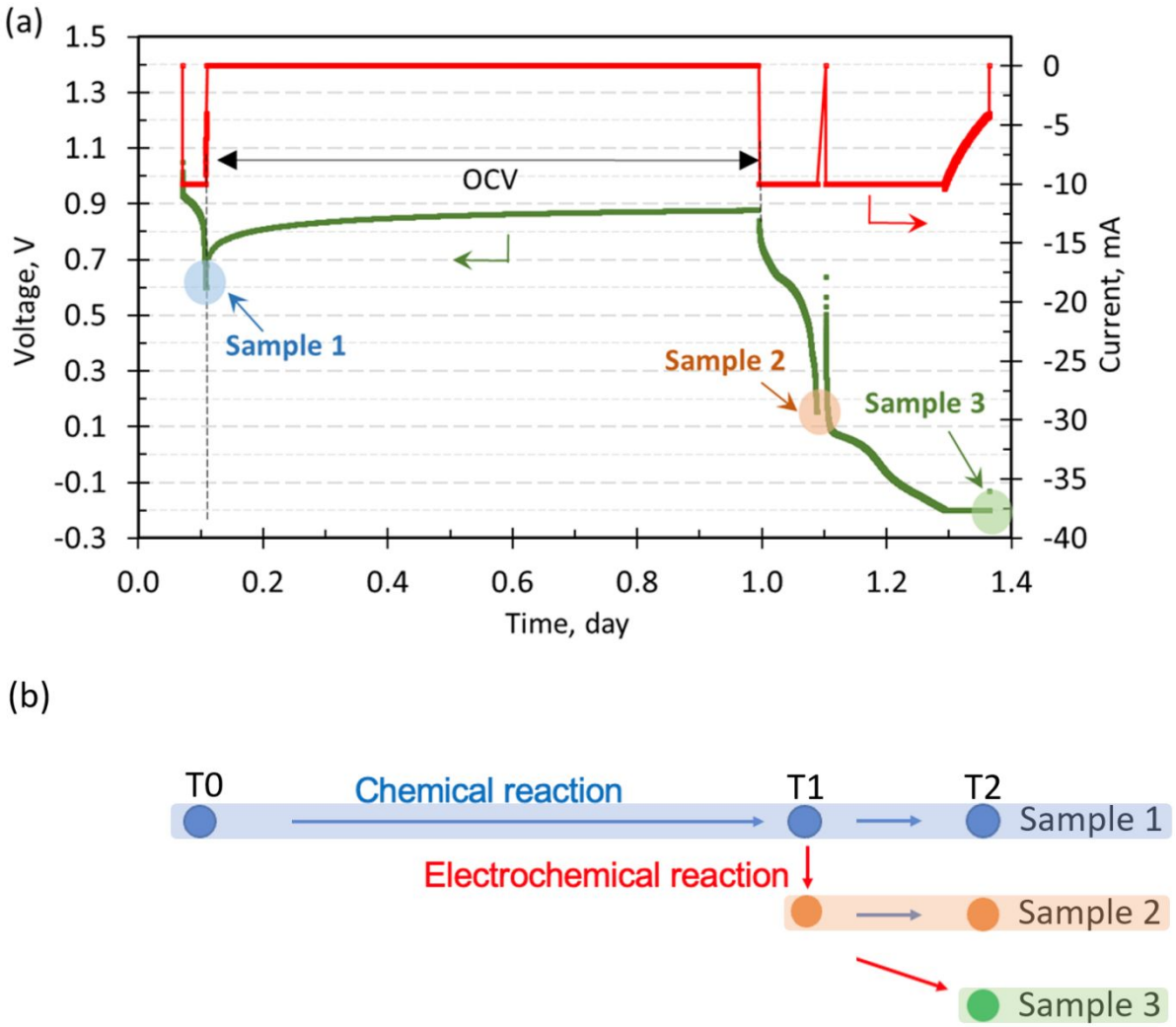

Figure S3. (a) Time-dependence of cell voltage and current during the conversion of DHA to DHAQ in a DHA | ferro/ferricyanide cell. (b) Reference for LC-MS samples. Test conditions: negolyte side contained 7.0-7.5 ml of 0.05 M DHA and the posolyte side consisted of 120 ml of 0.04 M potassium ferrocyanide and 0.02 M potassium ferricyanide in 2 M OH^-. DHA oxidation condition: constant current density at 2 mA/cm^2 followed by a potentiostatic hold at 0.6 V until a cutoff current density of 0.75 mA/cm^2. DHA dimer oxidation condition: constant current density at 2 mA/cm^2 followed by a potentiostatic hold at -0.2 V until a cutoff current density of 0.75 mA/cm^2. Subsequent cycling of the formed DHAQ was performed under constant current density

at 50 mA/cm^2 followed by a potentiostatic hold. The cutoff voltage for the charge and discharge steps were 1.4V and 0.95 V, respectively. Cutoff current densities for the charge and discharge steps were 2 mA/cm^2.

Three samples (aliquots) were taken from the negolyte at the times noted on Figure S3, set aside in a nitrogen-atmosphere glovebox and then were analyzed using LC-MS at various times. Sample 1, 2, and 3 were taken at T0 (when the oxidation of DHA was completed), T1 (a little after OCV step finished), and T2 (when the oxidation of the dimer was completed), respectively. Sample 1 was analyzed at T0, T1, and T2; Sample 2 was analyzed at T1 and T2; and finally, Sample 3 was analyzed at T2. Therefore, a total of six LC-MS tests were conducted and labeled as Sample 1_0, Sample 1_1, Sample 1_2, Sample 2_1, Sample 2_2, and Sample 3_2. The first numbers refer to the sample number, and the subscripts refer to the time when the sample was analyzed. For example, Sample 2_1 refers to Sample 2 analyzed at T2.

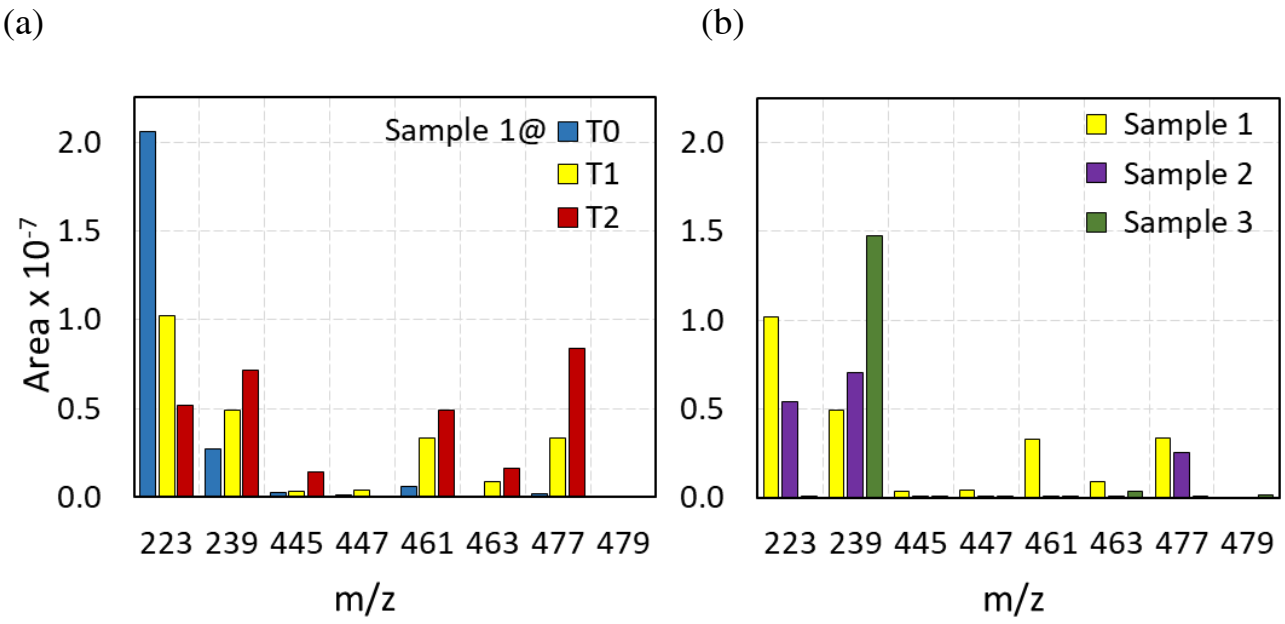

Figure S4. Absolute peak areas for species found in (a) Sample 1 at various times namely: Samples 1_0 (blue), 1_1 (orange), and 1_2 (green), and (b) in Samples 1_1, 2_1, and 3_2 through LC-MS analysis. The decimals are neglected for simplicity. Refer to Figure S3 for references to LC-MS samples.

Figure S4a shows the peak area of species in Sample 1 over time. The peak of the dimer decreases while new species gradually evolve, suggesting that the dimer convers to new species. The *m*/*z* of 223.04 and 239.03 refers to the dimer[3] and DHAQ, respectively. Notably, the peak intensity of DHAQ almost triples from T0 to T2. Other previously unexplored species that have *m*/*z* = 461.07 ($C_{28}H_{13}O_7$), 463.08 ($C_{28}H_{15}O_7$), and 477.08 ($C_{28}H_{15}O_8$) also grow. Because these new species have the same number of carbons but less hydrogens and more oxygens than the dimer ($C_{28}H_{18}O_6$), it seems that the dimer is oxidized. It should be mentioned that Sampe 1 does not undergo any further

electrochemical reaction; thus, the changes observed are caused solely by homogeneous chemical reaction(s).

Figure S4b shows the peak area of the species in Samples 1_1, 2_1, and 3_2. The changes observed are expected to be mainly due to the electrochemical processes involved from T1 to T2 (along the red arrows depicted on Figure S3b). The major changes from sample 1_1 to sample 2_1 are the shrinkage of peaks at m/z = 223.04 and 461.067 and a slight increase in peak intensity at 239.03. This result suggests that although the electrochemical oxidation from day 1 to 1.1 in Figure S3a enables the formation of DHAQ from the decomposed species (m/z = 461.07 and 477.08 to a lesser extent), the conversion is not complete. Based on Sample 3_2, during the electrochemical oxidation from day 1.1 to 1.4 in Figure S3a, the DHA dimer (m/z = 223.04) and also the compound at m/z = 477.08 are completely converted, and what is left is predominantly DHAQ (m/z = 239.03). The residual compounds (m/z = 463.08 and 479.08) imply that the regeneration process fails to convert all the dimer to DHAQ.

Section 4: NMR of Pristine DHAQ and DHAQ Oxidized at a Very Low Cell Voltage

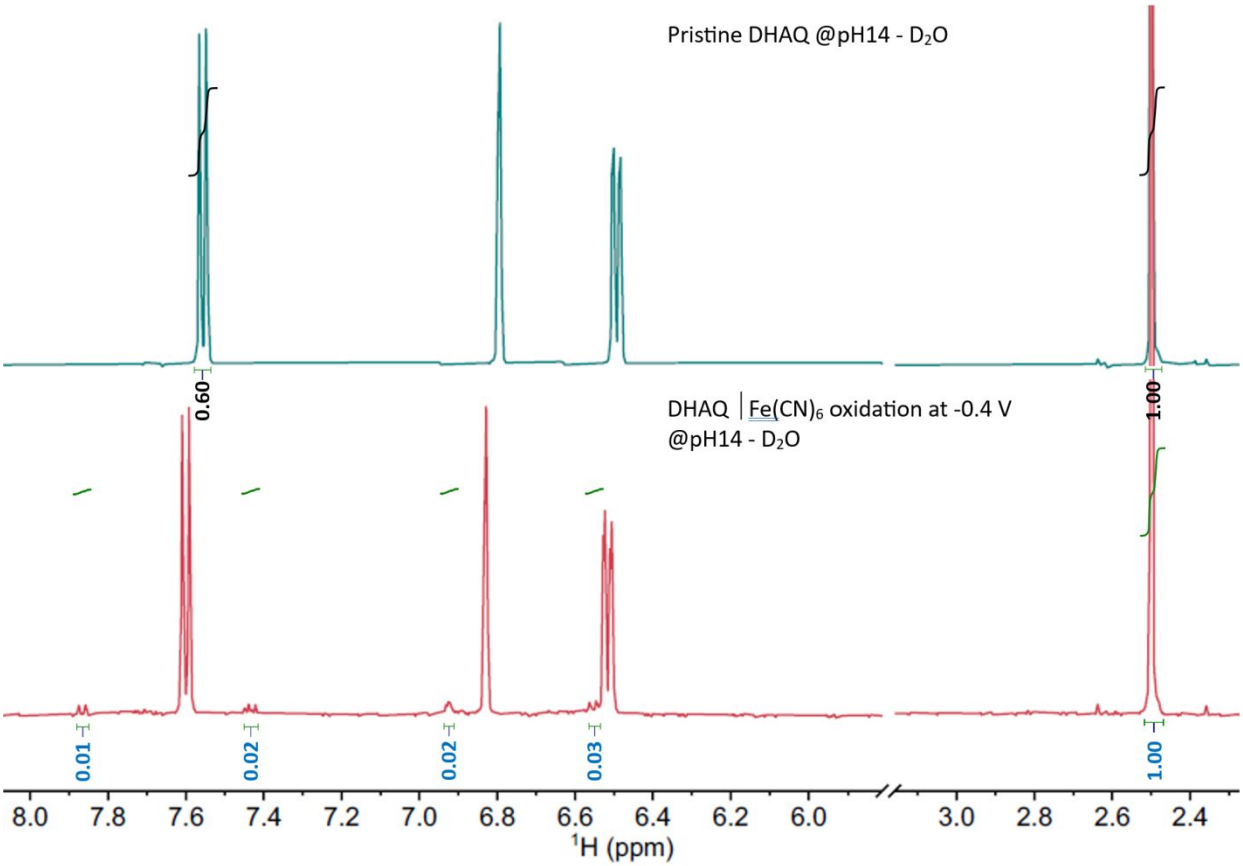

Figure S5. ^{1}H NMR spectrum of DHAQ under two conditions: pristine, and DHAQ oxidized at -0.4V cell voltage in a DHAQ | $K_4Fe(CN_6)$ flow cell both at pH14. To better present the peaks of interest, the solvent peak from D_2O is cut out. The peak at 2.5 ppm is from the internal standard of DMSO. The aromatic peaks of DHAQ in the second plot slightly shifted down fields, which is due to a slight pH change caused by the OER during the oxidation at -0.4V. The small peaks at 7.85, 7,45, 6.92, and 6.53 ppm in the bottom NMR spectrum are from the unidentified decomposition compounds generated during the oxidation at -0.4V.

Section 5: Energy Cost Analysis of the Regeneration Technique

Figure S6 shows the loss of energy efficiency and annual energy cost associated with performing regeneration steps at various OH^- concentrations. The annual energy cost decreases from ~ 20 to ~ 3 to Wh/L/year as the OH^- concentration increases to 2.0 M. The dependency on the OH^- concentration is indirect; the primary reason for the change in energy cost lies in the variation of the fade rate, necessitating different regeneration periods. Despite a higher annual energy cost in 1.0 M OH^-, the loss in energy efficiency is still very negligible and remains lower than 0.5%.

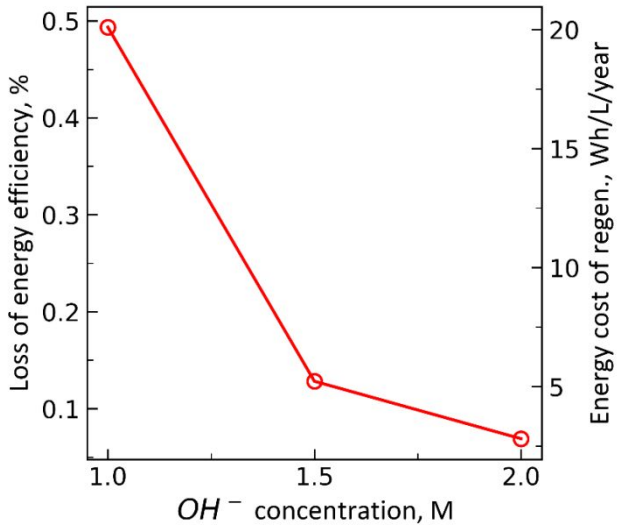

Figure S6. Loss of energy efficiency associated with performing regeneration steps and relevant energy costs at various OH^- concentrations.

The values in Figure S6 are based on the assumption that a regeneration step is initiated once a total fade of 5% in capacity is measured. Given the fade rates measured (and reported in Figure 5) for 0-85% cycling in 1.0 to 1.5, and 2.0 M OH^- concentrations, appropriate periods between

regeneration events are 0.24, 0.95, and 1.9 months (or a total of 50, 13, and 7 regenerations events in a year), respectively.

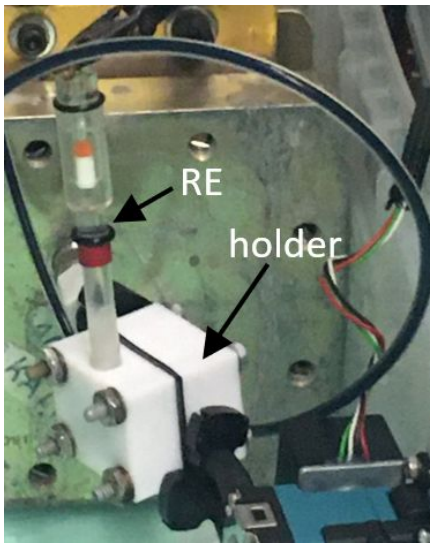

Figure S7. Placement of a reference electrode (RE) in a holder positioned on the inlet of the negolyte stream.

REFERENCES

(1) Ye, C.; Wang, A.; Breakwell, C.; Tan, R.; Grazia Bezzu, C.; Hunter-Sellars, E.; Williams, D. R.; Brandon, N. P.; Klusener, P. A.; Kucernak, A. R. Development of Efficient Aqueous Organic Redox Flow Batteries Using Ion-Sieving Sulfonated Polymer Membranes. *Nature communications* **2022**, *13* (1), 3184. DOI: 10.1038/s41467-022-30943-y.

(2) George, T. Y.; Thomas, I. C.; Haya, N. O.; Deneen, J. P.; Wang, C.; Aziz, M. J. Membrane–Electrolyte System Approach to Understanding Ionic Conductivity and Crossover in Alkaline Flow Cells. *ACS Applied Materials & Interfaces* **2023**, *15* (49), 57252-57264. DOI: 10.1021/acsami.3c14173.

(3) Goulet, M. A.; Tong, L.; Pollack, D. A.; Tabor, D. P.; Odom, S. A.; Aspuru-Guzik, A.; Kwan, E. E.; Gordon, R. G.; Aziz, M. J. Extending the Lifetime of Organic Flow Batteries Via Redox State Management. *J Am Chem Soc* **2019**, *141* (20), 8014-8019. DOI: 10.1021/jacs.8b13295.